Jurnal Kejuruteraan 38(5) 2026: 2383-2393
https://doi.org/10.17576/jkukm-2026-38(5)-23

Simulation-Based Structural Optimization of FBG-Integrated Stud Bolts for Real-Time Stress Monitoring in Flange Joints

Muhammad Abdullah[a], Mohd Hafizi Zohari[b*] & Ahmad Alias[c]

[a]*Advanced Structural Integrity and Vibration Research (ASIVR), Faculty of Mechanical & Automotive Engineering Technology, Universiti Malaysia Pahang Al-Sultan Abdullah (UMPSA), Malaysia,*

[b]*Centre for Advanced Industrial Technology, Universiti Malaysia Pahang, Al-Sultan Abdullah, 26600 Pekan, Pahang.*

[c]*Structural Performance and Materials Engineering Research (SUPREME), Universiti Malaysia Pahang, Al-Sultan Abdullah, 26600 Pekan, Pahang.*

[*]*Corresponding author: hafizi@umpsa.edu.my*

Received 13 August 2025, Received in revised form 6 May 2026
Accepted 5 June 2026, Available online 30 August 2026

ABSTRACT

In critical sectors such as oil and gas, more than 90% of bolted joint failures result from improper preload during installation. Loss of bolt tension can cause flange leakage, leading to environmental damage or fire hazards. This study aims to improve the performance of a modified M18 stud bolt integrated with Fiber Bragg Grating (FBG) sensors to reduce structural damage while enabling accurate real-time stress–strain monitoring. Finite Element Analysis (FEA) was conducted using ANSYS. Five bolt designs were evaluated under an applied torque of 70 Nm. The models varied in groove position to accommodate FBG sensor placement. Stress and strain responses were analyzed using a mesh size of 0.15 mm. The top groove extending to the flange end produced 2877.90 με strain but generated a maximum von mises stress of 582 MPa, approaching nearly the 640 MPa yield strength of Grade 8.8 steel. The centre groove extending to the flange end exceeded both 3000 με strain and the yield limit, indicating structural instability. In contrast, the top groove extending to the bolt end achieved 1639.5 με strain while maintaining a lower maximum stress of 323.04 MPa, well within the elastic range. Based on mechanical response and manufacturability considerations, the top groove till end configuration provides the most consistent balance between strain response and structural safety. The numerical results demonstrate that controlled groove placement enables strain sensing while preserving elastic behavior in bolted flange systems. The simulation confirms that this approach improves the safety of bolted flange systems and enables reliable real-time monitoring.

Keywords: FBG sensors; stud bolts health monitoring; strain transfer efficiency; sustainable flange joint integrity; bolt pre-load monitoring

INTRODUCTION

Bolted flange joints are essential in pipelines, chemical processing plants, power generation systems, and high-pressure vessels. Minor variations in bolt assembly can significantly affect operational safety and efficiency (Lu et al. 2024). These joints operate under cyclic pressure, thermal variation, and vibration (Mourya et al. 2015). Preload loss is the primary cause of joint failure. Most bolted joint failures result from incorrect tightening torque or joint separation during service (Michael 2021). Maintaining bolt integrity is therefore critical, as leakage can cause environmental damage or fire hazards (Cloostermans et al. 2025).

Strain gauges and ultrasonic sensors are commonly used to detect bolt preload but have practical limitations (Mayer et al. 2023). They require human intervention, are sensitive to temperature variation, and do not support continuous monitoring (Guo et al. 2022). In contrast, Fiber Bragg Grating (FBG) sensors provide a robust alternative. These optical sensors measure strain accurately and remain functional under severe thermal and environmental conditions (Yang et al. 2023). Their immunity to electromagnetic interference makes them well suited for flange environments with high industrial noise (Zhao et al. 2024).

Effective strain transmission depends on embedding FBG sensors within the bolt. Surface-mounted sensors often fail due to uneven stress distribution or adhesive degradation over time (Iwashita et al. 2024). Machining a groove in the bolt body to embed the sensor provides a direct and stable coupling to axial tension. This approach ensures accurate data acquisition and long-term stability (Rajabzadeh et al. 2018).

Groove design and placement strongly influence both the bolt stress field and the quality of strain transfer to the sensor. Central grooves disrupt load transmission and create stress concentrations that reduce bolt structural integrity (G. Guo et al. 2022). Prior studies show that off-axis channels near the bolt head preserve axial load paths and allow sensor integration without compromising structural performance (Iwashita et al. 2023).

Multiple real-world applications support this approach. In high-energy physics experiments, FBG sensors have been embedded in fragile mechanical components using shallow channels (Abdullah et al. 2025; Esposito, 2014). Experimental studies confirm that bolts with groove-embedded FBG sensors remain structurally robust while accurately measuring stress (Fan et al. 2023). Zhao et al. (2018) used finite element modeling to show that optimized groove geometry enables reliable stress monitoring without compromising mechanical strength.

FBG sensors are widely used for structural monitoring because they tolerate harsh environments and electromagnetic interference (EMI). They detect strain through shifts in the reflected light wavelength (Bhatti et al. 2024). In order to monitor structural components in real time, FBGs are implemented in the energy, aerospace, civil, and other multiple industries as well. (Hamza Siddique Bhatti et al. 2025).

Stress and preload loss are the primary causes of bolted joint failure. Conventional methods, such as strain gauges and torque-based monitoring, are intrusive and do not support continuous measurement (Samantaray et al. 2018). Embedding FBG sensors in bolts provides a compact, high-fidelity solution for continuous stress and strain monitoring in such applications (Chen et al. 2018).

The integration method of an FBG sensor strongly affects its performance. Surface-mounted FBG suffer from adhesion failure, thermal expansion mismatch, and delamination sensitivity (Guo et al. 2016). Studies show that embedding FBGs in short machined grooves improves adhesion and yields more accurate and reliable strain measurements (Iwashita et al. 2024).

(Zhao et al. 2018) demonstrated that selecting the groove strategically enhances stress distribution while maintaining structural integrity. Benussi et al. integrate FBGs into carbon fiber structures using machined space. They developed a design that maintained its stability over time and accurately measured strain as loads altered direction. This demonstrates that the groove method is effective for metal parts and bolts. (Benussi et al. 2015). Bhatti et al. discussed the long-term sustainability of FBGs in challenging environments, including areas with high levels of electromagnetic waves. (H. S. Bhatti et al. 2025).

Prabhugoud and Peters et al. use finite element models to examine bolts that were equipped with sensors. Their research showed that the structure remains durable and generates substantial strain differences that are advantageous for FBG interrogation due to the shallow, uneven grooves. This method is effective in accordance with the current practices in the design of SHM in aircraft and civil structures. (Prabhugoud & Peters 2006). Preciado et al. employed interferometers that were constructed with Bragg gratings to detect structural failures. Even when the stress was not evenly distributed, this method was effective. Embedded Bragg structures are suitable for use in fast-response tension systems due to their design concept. (Preciado et al. 2016).

To address this gap, this study numerically investigates multiple groove configurations machined into an M18 stud bolt using finite element analysis. The objective is to identify a groove location that enables effective strain transfer to an embedded FBG sensor while keeping induced stresses within allowable material limits under applied preload. The results support the rational design of FBG-embedded stud bolts for reliable preload monitoring in flange joint applications.

AXIAL PRELOAD–STRAIN RELATIONSHIP IN STUD BOLTS

Under elastic tightening, the applied torque T generates an axial preload F, which can be estimated using the torque–preload relationship. Here, D is the nominal bolt diameter (in mm), and K is the nut factor that accounts for the combined frictional resistance at the threads and under the bolt head. In this study, K is taken as 0.2 (Wu et al. 2020).

$$F = \frac{T}{KD}$$

For the applied torque of 70 Nm, using eq 1 the resulting axial preload is 19,444.44N≈ 19.44 kN This axial force was applied as the boundary load in the finite element simulations. The induced preload produces a uniform axial stress in the bolt shank given by:

$$\sigma = \frac{F}{A_{eff}} \quad (1)$$

where A_{eff} is the effective load-bearing cross-sectional area. Assuming linear elastic behavior, the corresponding axial strain is:

$$\varepsilon = \frac{\sigma}{E} = \frac{F}{A_{eff}E} \quad (2)$$

where E is Young's modulus of the bolt material.

For a homogeneous bolt without geometric discontinuities, the axial strain is uniform along the shank, enabling direct inference of preload from strain. However, introducing a groove modifies the local stiffness and effective area, producing non-uniform strain distributions. From a measurement perspective, this geometric perturbation must be carefully controlled to enhance strain sensitivity without violating elastic assumptions.

METHODOLOGY

A finite element–based numerical methodology was employed to evaluate the mechanical response of an FBG-integrated M18 stud bolt with different groove configurations under tightening preload. Five groove designs with varying axial locations along the bolt shank were modeled. The applied tightening torque was converted into axial preload and imposed on the bolt and flange assembly. Stress and strain responses were extracted from the groove regions to assess strain transfer suitability for FBG sensing while ensuring structural safety of the bolt.

A standard M18 stud bolt was selected because of its widespread use in industrial flange joints. The bolt was numerically modeled using carbon steel Grade 8.8, with an elastic modulus of 210 GPa and a yield strength of 640 MPa. The nominal diameter was 18 mm, and the total length was 125 mm (Kodur et al. 2017). Five bolt configurations were analyzed. The baseline model had no groove. The remaining four models included grooves located either along the top or the central axis. Two groove configurations extended along the full bolt length, while the other two terminated at the flange end.

The groove width could not be expanded beyond its current dimensions due to sensor and machining limitations. The groove's dimensions were 4 mm in width, while the depth was 3.5 mm. They were directed by the sensor implantation guidelines established by prior experimental and simulation studies . (Zhao et al. 2018) demonstrated that the sensor is not subjected to excessive strain and that strong bonding is facilitated by the presence of inverted grooves of the same dimension.

TABLE 1. Summary of groove configurations evaluated in the study.

Configuration ID	Groove Location	Groove Configuration
G0	No groove	Without any groove
G1	Centre groove	Centre Groove till end
G2	Top groove	Top Groove till end
G3	Centre groove	Centre Groove till flange end
G4	Top groove	Top Groove till flange end

The bolts were modeled in 3D modeling software and then imported into ANSYS Workbench. The structure was generated using tetrahedral elements (SOLID187) and a uniform element size of 0.15 mm. Each model generated approximately 35000 to 41000 nodes and more than 72,000 elements. A uniform element size was used throughout the model. The groove tips and groove boundaries were inspected to confirm that the mesh adequately resolved the stress/strain gradients in that region. The goal of this simulation was to address stress accumulation at groove corners and ensure that the designs maintained a consistent level of precision.

Boundary conditions replicate a stud bolt on flange joint loading. The boundary conditions of the bonded bolt were as follows: the x and z displacements were restrained; a fully fixed bottom surface; and the groove and top surfaces were free. A tightening torque of 70 Nm was converted to an axial preload (19.44 kN) and applied as the axial load in the FEA. Axial preload was applied to the opposite end (Zhao et al. 2018). The torque measurements had been converted into axial force by using equation 1.

Figure 1 illustrates the boundary conditions used in the FEA simulation. The bolt–flange assembly is constrained to eliminate rigid body motion, and the applied tightening torque is converted into an equivalent axial preload along the bolt axis. This setup represents typical flange tightening conditions and allows consistent comparison across groove configurations.

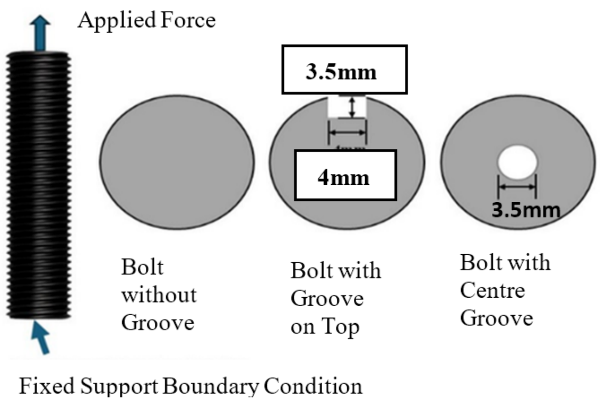

FIGURE 1. Boundary conditions in the FEA simulation

The simulations provided mainly two primary outputs, which are Equivalent von-mises Stress (MPa), Equivalent Elastic Strain (με), which basically provide the von mises stress distribution and the equivalent elastic strain across the bolt. The stress field enabled the assessment of structural stability (Wang et al. 2021). The quality of the sensor signal anticipated at various groove locations was indicated by the strain data. The simulation also assessed the uniformity of stress at the groove boundaries. This parameter was crucial, as the probability of fatigue failure is elevated by unexpected gradients. This method is consistent with the technique outlined by (Zhao et al. 2018), who optimized groove bonding for FBG sensor placement by simulating similar bolts under static axial load.

The models were compared to determine which groove design achieved the highest strain transmission without exceeding the bolt material's yield strength limit. Utilizing the modeling methodology and analysis techniques, the structural feasibility of sensor-embedded bolt designs was evaluated with great precision and consistency.

Figure 2 shows the three-dimensional finite element model of the M18 stud bolts, and Table 1 summarizes the positioning of the five groove configurations evaluated in this study. The model includes the threaded region, shank, and groove locations along the bolt axis. These configurations form the basis for assessing the effect of groove position on stress and strain distributions under tightening preload.

FIGURE 2. Configurations of all groove designs placement on bolts

The present study is based exclusively on numerical simulations. No physical fabrication or experimental testing of the stud bolts was performed. The numerical results are evaluated by comparison with established trends and benchmark values reported in the literature for carbon steel Grade 8.8 bolts under preload conditions

SIMULATION AND ANALYSIS

The simulations were conducted on five different configurations of M18 stud bolts to determine the impact of various grooves on the structural health of the M18 stud bolt. These models were subjected to axial loading that simulated a variety of real-world flange joint configurations.

The goal was to comprehend the impact of groove location and length on internal stress distribution and strain transfer, which are essential for the performance of sensors and the integrity of bolts. The simulations offered a precise understanding of the manner in which each groove variant interacts with preload forces throughout the length of the bolt, as opposed to relying on assumptions. This method facilitated a systematic comparison that was based on actual mechanical behavior rather than theoretical approximation. The following figures below present the finite element contour results for each bolt configuration under a tightening torque of 70 Nm

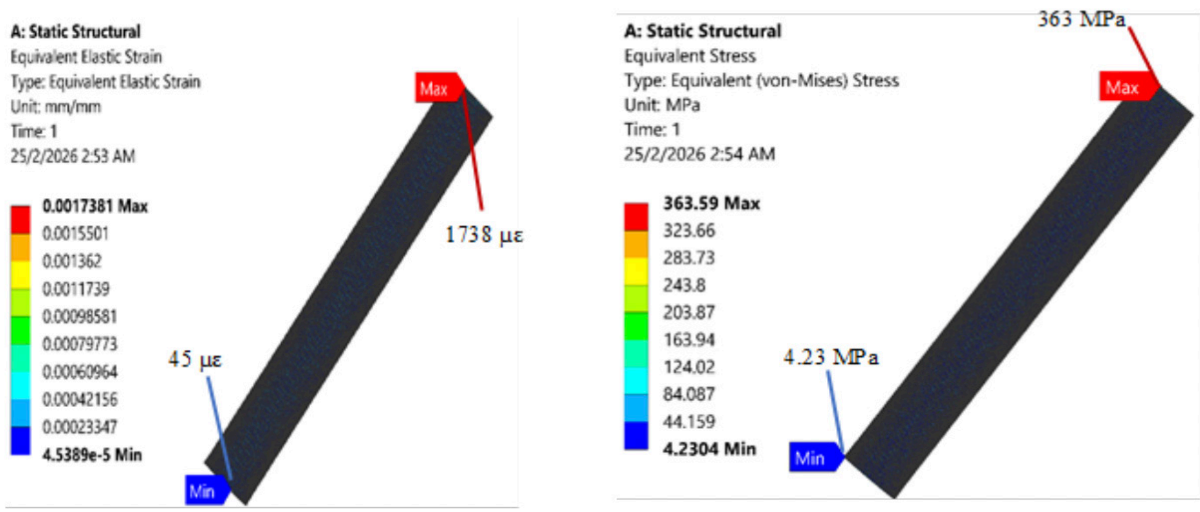

(a) (b)

FIGURE 3. (a) Equivalent elastic strain (με) and (b) von mises stress (MPa) distributions in the G0 configuration.

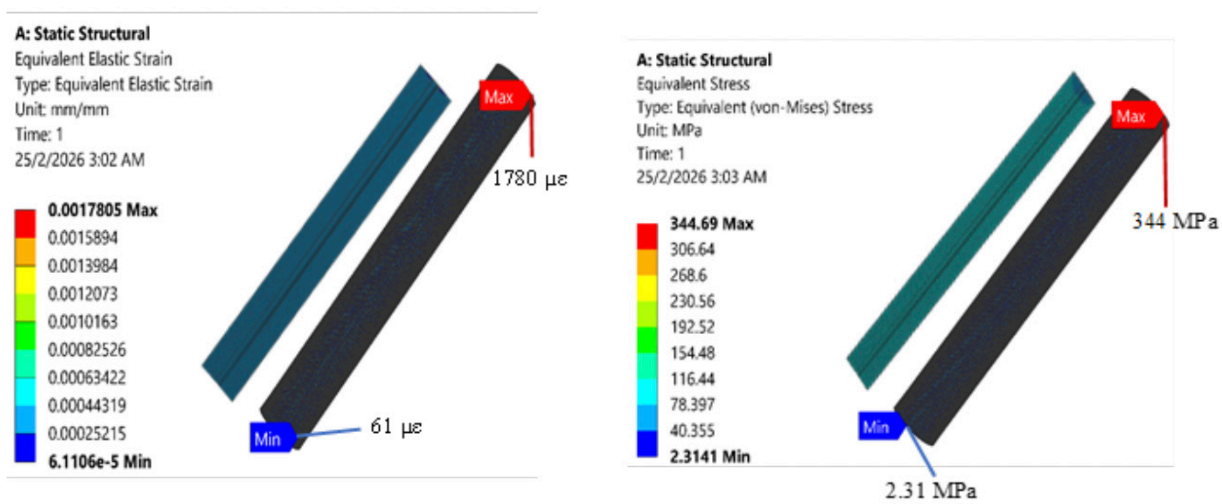

(a) (b)

FIGURE 4. (a) Equivalent elastic strain (με) and (b) von mises stress (MPa) distributions in the G1 configuration.

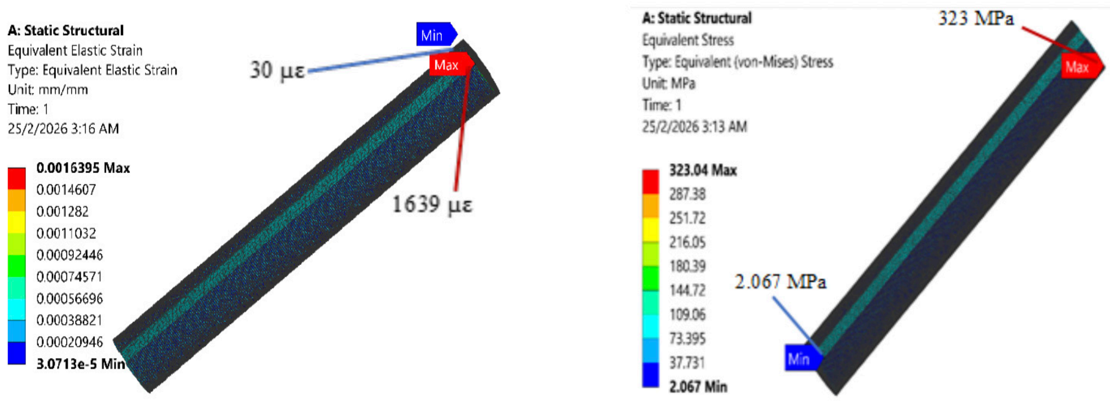

(a) (b)

FIGURE 5. (a) Equivalent elastic strain (με) and (b) von mises stress (MPa) distributions in the G2 configuration

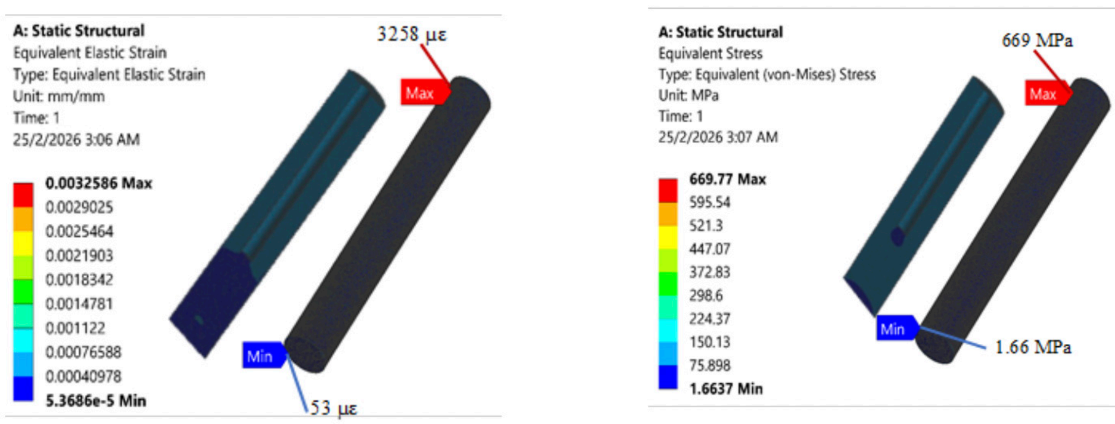

(a) (b)

FIGURE 6. (a) Equivalent elastic strain (με) and (b) von mises stress (MPa) distributions in the G3 configuration

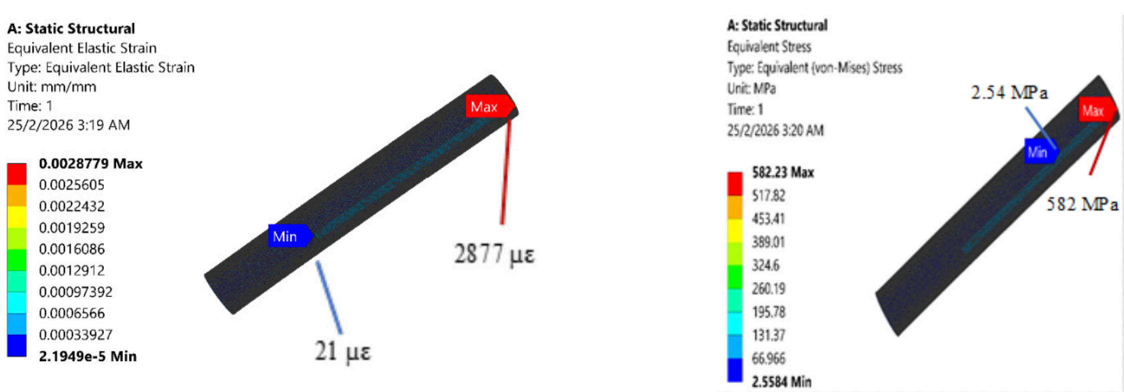

(a) (b)

FIGURE 7. (a) Equivalent elastic strain (με) and (b) von mises stress (MPa) distributions in the G4 configuration

Figures 3–7 present the finite element contour distributions of equivalent elastic strain and von mises stress for five bolt configurations under 70 Nm torque. Each figure presents the three-dimensional stress and strain contours, with the corresponding maximum and minimum values clearly marked. The contours display axial strain in the groove region and stress distribution along the bolt shank under identical preload conditions. All configurations use the same material properties, boundary conditions, and loading parameters to enable consistent comparative evaluation of the results.

The simulated stress and strain distributions for grooved stud bolts are consistent with established findings in bolted joint mechanics and sensor integration studies. Finite element modelling of preloaded bolted connections has been shown to accurately predict stress–strain behavior when 3D solid models are used (Kim et al. 2007), and stress concentrations arising from geometric discontinuities such as grooves align with documented optimization trends in bolted joints (Croccolo et al. 2023). The observed increase in localized strain with extended groove length is supported by published analyses of strain transfer mechanisms in embedded FBG sensors, which demonstrate that sensor location and structural modification significantly influence strain capture (Kerrouche et al. 2009). Experimental work on M18 studs instrumented with FBG sensors further confirms the direct relationship between preload and measured strain response(Abdullah et al. 2025) (Adhreena & Hafizi, 2023). Additionally, finite element studies of pre-tightening processes show that torque–preload relationships produce stress distributions consistent with those predicted in this work (Yu & Zhou, 2015). These literature-supported trends validate the interpretation of simulation results in the present study.

DISCUSSION

From an instrumentation and measurement standpoint, the objective of an FBG-embedded bolt is stable and repeatable strain transfer within the elastic regime of the host structure. Exceeding yield introduces nonlinear deformation, residual strain, and hysteresis, which degrade the wavelength-based strain interpretation fundamental to FBG sensing.

The findings derived from numerical simulations were validated by the examination of stress and strain contours. The positioning of the top groove led to smoother deformation, which in turn reduced the sharpness of stress differences. These smoother profiles are well-established research that underscores the advantages of off-axis groove placements in terms of preserving axial rigidity while simultaneously facilitating strain capture (Zhang et al. 2024). The simulation analysis demonstrated the impact of the groove design on the structural health of the bolt and the accuracy of the sensor.

The smoother stress and strain distributions are important for long-term sensing stability. Reduced stress gradients reduce the risk of sensor detachment and improve the consistency of strain measurements under load variation. This improves the correlation between FBG strain readings and bolt preload, supporting dependable long-term monitoring of flange joints. These outcomes indicate that groove optimization should be treated as a core measurement-system design step rather than a purely mechanical modification. Maximizing strain output alone is insufficient; safe and linear elastic operation is essential for accurate and repeatable preload measurement.

TABLE 2. Comparison Study of the results of parameters under 70Nm Torque

Bolt Configuration	Bolt Design	Equivalent von-mises Stress (MPa)	Equivalent Elastic Strain (με)
		(Max)	(Max)
G0	Bolt Without Groove	363.59	1738.2
G1	Bolt with Centre Groove till End	344.69	1780.5
G2	Bolt with Top Groove till End	323.04	1639.5
G3	Bolt with Centre Groove till Flange End	669.77	3258.6
G4	Bolt with Top Groove till Flange End	582.23	2877.9

According to Table 2, stable mechanical behavior was demonstrated by the standard bolt (G0) model without any groove. It had a strain output of 1738.2 με and the lowest von mises stress of 363.59 MPa. The ungrooved design served as the structural benchmark. However, it cannot accommodate an embedded sensor, limiting its applicability for real-time monitoring.

The introduction of top groove extending along the full bolt length (G2) produced a strain of 1639.5 με. The corresponding von mises stress reached 323.04 MPa, which remains well below the 640 MPa yield strength of carbon steel Grade 8.8. Although this configuration does not violate the elastic limit, the increase in localized stress relative to the ungrooved bolt indicates reduced stress margin under preload. The design enhances strain response while maintaining elastic behavior; however, stress concentration near the groove boundaries warrants consideration under cyclic or variable loading conditions.

The top groove extending to the flange end (G4) produced a peak strain of 2877 με, indicating high-strain sensitivity. The corresponding maximum von mises stress reached 582.23 MPa, remaining below but approaching the yield strength of carbon steel Grade 8.8.

Top-grooved configurations (G2 & G4) preserve the primary axial load bearing core by shifting the groove away from the maximum axial stress region. The full-length top groove produced relatively low peak stress with measurable strain, suggesting improved mechanical robustness.

The structural response was changed when a centre groove till end (G1) was introduced. The strain reached 1780.5 με, and the stress values increased to 344.69 MPa. The central groove disrupted the load path along the bolt's neutral axis, even though these values were within acceptable limits. The G1 configuration increases axial strain relative to the ungrooved bolt while keeping von mises stress below the 640 MPa yield strength of Grade 8.8 steel. The groove reduces effective load-bearing area along the primary load path, increasing local stress concentration and modifying axial stiffness.

The centre groove till flange end (G3) configuration produced the highest strain, 3258.60 με, indicating increased local compliance. It also generated the highest von mises stress, 669.77 MPa, exceeding the 640 MPa yield strength of carbon steel Grade 8.8.

Grooves till flange end designs (G3 & G4) increase the measured strain (higher sensitivity), they also introduce pronounced stress concentrations near the groove termination and flange interface. In particular, the centre-groove till flange end configuration exceeds the yield limit. This stress increase results from reduced effective cross-sectional area and the abrupt geometric transition at the groove termination, which intensifies stress concentration under preload. Exceeding the yield limit induces localized plastic deformation and permanent strain, eliminating elastic behavior. The resulting plastic zones reduce load-carrying capacity and safety margin, thereby making the design structurally unstable for practical application because it violates the linear strain–wavelength assumption and reduces long-term structural reliability despite its high strain response.

The centre groove till end and top groove till end (G1 & G2) configurations produce comparable strain; however, the top groove (G2) generates lower peak von mises stress under identical preload. From a manufacturing standpoint, a surface top groove is simpler and more controllable than drilling an internal axial bore, which requires additional operations and tighter tolerances. Lower machining complexity reduces the risk of geometric defects that can intensify stress concentration. Considering both mechanical response and manufacturability, the top groove configuration may therefore be preferred for practical implementation.

Controlled groove placement enables reliable strain measurement while maintaining the mechanical integrity of the bolt under preload. Among the configurations evaluated, top grooves demonstrate the most favorable balance between strain response and structural performance, supporting their suitability for real-time stress monitoring in flange joint application.The predicted stress levels and strain distributions agree with previously reported numerical and experimental results for carbon steel Grade 8.8 bolts under tightening preload, including those of Kodur et al. (2017), supporting the validity of the simulations.

Figure 8 quantitatively compares the maximum von mises stress and equivalent elastic strain for all five bolt configurations under a tightening torque of 70 Nm. The graph provides a direct numerical assessment of the mechanical response associated with each groove geometry, enabling evaluation of stress magnitude relative to material yield strength and corresponding strain levels relevant to sensing performance.

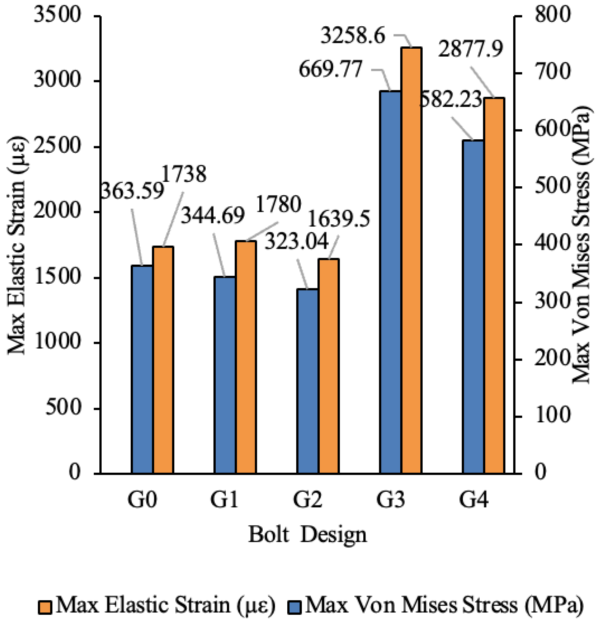

FIGURE 8. Comparison of von mises stress and strain of all groove designs

As figure 8 shows the maximum von mises stress and equivalent elastic strain for all configurations under 70 Nm torque, highlighting the mechanical response associated with each groove geometry. Among the evaluated designs, the top groove till end (G2) configuration exhibits a high strain response while maintaining stress levels within the elastic range relative to the 640 MPa yield strength of Grade 8.8 steel. This indicates a controlled stress state with an acceptable safety margin under preload. The quantitative values summarized in Table 1 further confirm that this configuration provides a consistent balance between strain response and structural integrity, supporting its suitability for subsequent experimental validation and application in flange joint monitoring systems.

LIMITATION

This study is limited to static preload conditions and does not explicitly model cyclic fatigue, thermal gradients, corrosion, or manufacturing tolerances. The adhesive layer and sensor–substrate interface were not explicitly represented as separate materials, which may affect absolute strain transfer in practice. Nevertheless, the static stress/strain state provides a necessary baseline for identifying mechanically safe groove placement prior to experimental validation and durability testing.

CONCLUSION

This study evaluated five groove configurations in M18 stud bolts using finite element analysis under 70 Nm torque to assess strain response and structural integrity for FBG integration. The ungrooved bolt (G0) maintained uniform stress but could not accommodate a sensor. The centre groove till end (G1) configuration increased strain while remaining very close to the 640 MPa yield strength; however, alignment with the primary load path reduced axial stiffness and increased stress concentration, lowering structural margin under preload variation. It also requires internal boring and tighter geometric control, increasing manufacturing complexity.

Grooves extending to the flange end (G3 & G4) produced strain above 3000 με but exceeded the yield limit, causing plastic deformation and eliminating elastic behavior, which precludes practical use. The top groove till end configuration (G2) generated 1639.5 με strain with a maximum von mises stress of 323 MPa, well within the elastic range. It preserved axial load transfer, maintained structural margin, and allowed simpler surface machining. Based on mechanical response and manufacturability, the top groove till end configuration provides the most mechanically stable option for experimental validation and real-time monitoring.

ACKNOWLEDGEMENT

The authors gratefully acknowledge the Research and Innovation Department of Universiti Malaysia Pahang Al-Sultan Abdullah (UMPSA) for supporting this work through the internal research grant (Grant No. RDU233005).

DECLARATION OF COMPETING INTEREST

None.

REFERENCES

Abdullah, M., Zohari, M. H., Ramli, R., Muhammad Shukri, N. A. A. & Priyandoko, G. 2025. Investigation of stud bolts with incorporated fiber Bragg grating sensors for real-time flange bolt integrity monitoring. *Journal of Advanced Research in Applied Mechanics* 141(1): 148–162. https://doi.org/10.37934/aram.141.1.148162

Adhreena, M. S. N. A. & Hafizi, Z. M. 2023. A review on the application of fiber Bragg grating sensors in bolted joints health monitoring. In *Technological Advancement in Instrumentation & Human Engineering*, edited by Hassan, M. H. A., Zohari, M. H., Kadirgama, K., Mohamed, N. A. N. & Aziz, A., 655–667. Singapore: Springer Nature Singapore.

Benussi, L., Bianco, S., Caponero, M., Muhammad, S., Passamonti, L., Piccolo, D., Pierluigi, D., Raffone, G., Russo, A. & Saviano, G. 2015. Fiber Bragg grating sensors for deformation monitoring of GEM foils in HEP detectors. *2015 6th International Workshop on Advances in Sensors and Interfaces (IWASI)*, 75–78. https://doi.org/10.1109/IWASI.2015.7184954

Bhatti, H. S., Abdullah, M. A., Hadeed, M., Epin, V., Mohamad, H. & Lim, K.-S. 2025. Highly sensitive fiber Bragg grating geophone for low-frequency seismic detection. *IEEE Transactions on Instrumentation and Measurement* 74: 1–7. https://doi.org/10.1109/TIM.2025.3545528

Bhatti, H. S., Aizzuddin, A. M., Hadeed, M., Vorathin, E. & Mohamad, H. 2024. Review of fibre optic geophones and accelerometers for potential application in seismic acquisition for carbon storage monitoring. *Optics & Laser Technology* 179: 111368. https://doi.org/10.1016/j.optlastec.2024.111368

Bhatti, H. S., Aizzuddin, A. M., Hadeed, M., Vorathin, E., Mohamad, H. & Lim, K. S. 2025. Temperature and chirp compensated fibre Bragg grating geophone for improved seismic detection. *Optics Communications* 579: 131533. https://doi.org/10.1016/j.optcom.2025.131533

Chen, D., Huo, L., Li, H. & Song, G. 2018. A Fiber Bragg Grating (FBG)-enabled smart washer for bolt pre-load measurement: Design, analysis, calibration, and experimental validation. *Sensors* 18: 2586. https://doi.org/10.3390/s18082586

Cloostermans, B., Pronk, D., Bruckenburg, B., Goossens, S., Baghdasaryan, T. & Berghmans, F. 2025. Bolted flange connection leakage: A systematic review of monitoring challenges and technologies. *IEEE Sensors Reviews* 2: 1–16. https://doi.org/10.1109/SR.2025.3550861

Croccolo, D., De Agostinis, M., Fini, S., Khan, M. Y., Mele, M. & Olmi, G. 2023. Optimization of bolted joints: A literature review. *Metals* 13(10): 1708. https://doi.org/10.3390/met13101708

Esposito, M. 2014. *Fiber Optical Sensors for High Energy Physics*.

Fan, J., Yuan, Q., Wei, L., Zhang, L., Zhang, D., Zhang, D. & Wang, Y. 2023. Experimental study of anchor bolt stress evaluation with hybrid optical fiber monitoring. *Optical Fiber Technology*: 103415. https://doi.org/10.1016/j.yofte.2023.103415

Guo, G., Zhang, D., Duan, Y., Zhang, G. & Chai, J. 2022. Strain-sensing mechanism and axial stress response characterization of bolt based on fiber Bragg grating sensing. *Energies* 15: 6384. https://doi.org/10.3390/en15176384

Guo, Y., Kong, J., Liu, H., Hu, D. & Qin, L. 2016. Design and investigation of a reusable surface-mounted optical fiber Bragg grating strain sensor. *IEEE Sensors Journal* 16: 8456–8462. https://doi.org/10.1109/JSEN.2016.2614009

Iwashita, W., Matsuakwa, H. & Otsuki, M. 2023. Control of static friction by designing grooves on friction surface. https://doi.org/10.21203/rs.3.rs-3356991/v1

Iwashita, W., Matsukawa, H. & Otsuki, M. 2024. Control of static friction by designing grooves on friction surface. *Tribology Letters* 72(1): 25. https://doi.org/10.1007/s11249-023-01822-4

Kerrouche, A., Boyle, W. J., Sun, T., Grattan, K. T., Schmidt, J. W. & Taljsten, B. 2009. Strain measurement using embedded fiber Bragg grating sensors inside an anchored carbon fiber polymer reinforcement prestressing rod for structural monitoring. *IEEE Sensors Journal* 9(11): 1456–1461.

Kim, J., Yoon, J.-C. & Kang, B.-S. 2007. Finite element analysis and modeling of structure with bolted joints. *Applied Mathematical Modelling* 31(5): 895–911.

Kodur, V., Yahyai, M., Rezaeian, A., Eslami, M. & Poormohamadi, A. 2017. Residual mechanical properties of high strength steel bolts subjected to heating-cooling cycle. *Journal of Constructional Steel Research* 131: 122–131. https://doi.org/10.1016/J.JCSR.2017.01.007

Lu, X., Zhu, M., Wang, S., Li, S., Xu, Z. & Liu, Y. 2024. Progress in theoretical modelling of macroscopic and microscopic dynamics of bolted joints in complex equipment. *Lubricants* 12(5): 182. https://doi.org/10.3390/lubricants12050182

Mayer, J., Klumpp, V., Hillenbrand, J. & Noack, B. 2023. Statistical approach for preload monitoring of ball screw drives. *2023 IEEE SENSORS*, 1–4. https://doi.org/10.1109/SENSORS56945.2023.10325060

Michael, W. 2021. Bolted joint preload distribution from torque tightening. *Strojnícky Časopis — Journal of Mechanical Engineering* 71: 329–342. https://doi.org/10.2478/scjme-2021-0039

Mourya, R. K., Banerjee, A. & Sreedhar, B. K. 2015. Effect of creep on the failure probability of bolted flange joints. *Engineering Failure Analysis* 50: 71–87. https://doi.org/10.1016/j.engfailanal.2015.01.005

Prabhugoud, M. & Peters, K. 2006. Finite element model for embedded fiber Bragg grating sensor. *Smart Materials and Structures* 15: 550–562. https://doi.org/10.1088/0964-1726/15/2/038

Preciado, M. A., El-Taher, A., Shu, X. & Sugden, K. 2016. Distributed delay-line interferometer based on a Bragg grating in transmission mode. https://doi.org/10.48550/arXiv.1611.06794

Rajabzadeh, A., Heusdens, R., Hendriks, R. & Groves, R. 2018. Calculation of the mean strain of smooth non-uniform strain fields using conventional FBG sensors. *Journal of Lightwave Technology* PP. https://doi.org/10.1109/JLT.2018.2849212

Samantaray, S., Mittal, S., Mahapatra, P. & Kumar, S. 2018. An impedance-based structural health monitoring approach for looseness identification in bolted joint structure. *Journal of Civil Structural Health Monitoring* 8: 809–822. https://doi.org/10.1007/S13349-018-0307-2

Wang, Y.-Z., Li, G., Wang, Y.-B. & Lyu, Y. 2021. Simplified method to identify full von Mises stress-strain curve of structural metals. *Journal of Constructional Steel Research* 181: 106624. https://doi.org/10.1016/J.JCSR.2021.106624

Wu, Z., Zhang, G., Du, W., Wang, J., Han, F. & Qian, D. 2020. Torque control of bolt tightening process through adaptive-gain second-order sliding mode. *Measurement and Control* 53(7–8): 1131–1143.

Yang, W.-S., Chiang, C. & Hsu, H.-C. 2023. Monitoring torque in bolts using an embedded fiber Bragg grating sensor. *Optik*: 171294. https://doi.org/10.1016/j.ijleo.2023.171294

Yu, Q. & Zhou, H. 2015. Finite element study on pre-tightening process of threaded connection and failure analysis for pressure vessel. *Procedia Engineering* 130: 1385–1396.

Zhang, N., Luo, B., Huang, L. & Luo, M. 2024. Research on the anti-slip performance of arc groove cable clamps. *Journal of Constructional Steel Research*: 108858. https://doi.org/10.1016/j.jcsr.2024.108858

Zhao, J., Dong, W., Hinds, T., Li, Y., Splain, Z., Zhong, S., Wang, Q., Bajaj, N., To, A., Ahmed, M., Petrie, C. M. & Chen, K. P. 2024. Embedded Fiber Bragg Grating (FBG) sensors fabricated by ultrasonic additive manufacturing for high-frequency dynamic strain measurements. *IEEE Sensors Journal* 24(3): 2853–2862. https://doi.org/10.1109/JSEN.2023.3343604

Zhao, Y., Zhang, N., Si, G. & Li, X. 2018. Study on the optimal groove shape and glue material for fiber Bragg grating measuring bolts. *Sensors* 18: 1799. https://doi.org/10.3390/s18061799